SF2A 2012
S. Boissier, P. de Laverny, N. Nardetto, R. Samadi, D. Valls-Gabaud and H. Wozniak (eds)

JUPITER SYNCHROTRON IMAGING WITH LOFAR

J. N. Girard[1], P. Zarka[1], C. Tasse[2], S. Hess[3] and the LOFAR Collaboration

Abstract. Since its detection in the mid-fifties, the synchrotron radiation, emitted by the Jupiter radiation belts at decimeter wavelengths ("DIM"), has been extensively observed over a wide spectrum (from >300 MHz to 22 GHz) by various instruments (VLA, ATCA, WSRT). They provided accurate flux measurements and resolved images of the emission that reveal spatial, temporal and spectral variabilities. However, no instrument was able to image the radiations belts below 100 MHz (at meter and decametre wavelength). The LOw Frequency ARray (LOFAR) (van Haarlem et al. 2012), which is a phased-array interferometer operating in the [30-80] & [110-250] MHz bandwidth, observed for the first time the Jupiter synchrotron emission. The antenna distribution provided baselines from 70 m up to ∼20 km that resolved the emission at low frequencies (127-172 MHz) during its commissioning phase. In November 2011, a single 10-hour track enabled to cover an entire planetary rotation in a bandwidth of 24 MHz. We present here the specific methods and steps implemented to reduce and to image the planetary data at low frequencies. At this stage of the commissioning, the smoothness of the synchrotron spectrum enabled the direct comparison between the expected flux density and the measurements from VLA data obtained in 1994 and 1998 (Kloosterman et al. 2008). We measured a total flux density of $3.5 - 4 \pm [0.1 - 0.3]$ Jy, slightly lower to what was obtained from VLA observations and models ($\sim 5 - 6$ Jy). Future joint observations that cover the whole spectrum of the emission will enable the tracking of its temporal short- and long-term variability. The study of this variability brings information about the source, loss and transport processes taking place in the inner Jovian magnetosphere, improving in the same time the existing radiative code and magnetospheric models.

Keywords: Jupiter, synchrotron emission, LOFAR, low frequency radioastronomy.

1 Radio emissions at Jupiter

1.1 Various sources of radio emissions

The giant magnetized planet Jupiter is known to be a strong source of radio emissions from few kHz to few hundreds of GHz (Dessler 2002a; Zarka 2004). These radio emissions have three main components. The most powerful comes from the sporadic bursts of (non-thermal) emissions ($> 10^7$ Jy[i]) below 40 MHz in the decametre (DAM) range (Burke & L. 1955; Zarka 2004). Accelerated electrons (of energy $E \sim$ keV) emit radio waves at the local cyclotron frequency presumably by the non-linear wave-particle interactions known as the "Maser Cyclotron Instability" mechanism (Treumann 2006; Wu & Lee 1979).
The second radio emission dominates in the dm-cm range (DIM) and is associated to relativistic motion of high-energy electrons (from E≈100 keV to MeV Mayer et al. (1958)). They emit at the local synchrotron frequency in the vicinity of Jupiter radiation belts (forming Van Allen belts analog to Earth belts).
The third radio component is the thermal emission from the planet atmosphere which dominates above 5 GHz. These components are depicted on Fig. 1 (left) from (Zarka 2004).

[1] LESIA, Observatoire de Paris, CNRS, UPMC, Université Paris-Diderot, 5 place Jules Janssen, 92195 Meudon, France
[2] GEPI, Observatoire de Paris, CNRS, 92195 Meudon, France
[3] LATMOS/IPSL, OVSQ, Guyancourt, France
[i] 1 Jy= 10^{-26} W.m^{-2}.Hz^{-1}

1.2 Synchrotron emission & previous observations

The relativistic electrons radiate synchrotron radio waves as they travel along a helix with a "pitch angle" α in the inner magnetic field $\vec{B}$ of the planet. This results in a collimated forward emission with a beaming angle $\theta_b \propto \frac{2}{\Gamma}$ with Γ the Lorentz factor of the electrons. From Dessler (2002b), it has the following characteristics:

- This synchrotron radiation shows a high level of linear polarization (of order 20%) and a low level of circular polarization (≈1%). The polarization direction is nearly orthogonal to that of $\vec{B}$.
- Along with source and loss processes occurring between the electrons and the ionosphere, the satellites and the dust, the sources of emission are closely confined to the planet in the plane of the magnetic equator (Roberts 1976) perpendicular to the planet magnetic moment. They form a donut-like belt around the planet that extends from 1.6 to 3 R_j (with R_j the Jupiter radius).
- The emission is optically thin and therefore the radio emission seen by a remote observer accumulates on both sides of the planet in the magnetic equator and forms two radiation peaks at low Jovian latitudes. Another component exists at higher magnetic latitudes ($\approx \pm 35^o$) in both hemisphere and originates from electrons populations having a different value of the pitch angle. The separation between low and high magnetic latitudes sources is due to the interaction of electrons with Jovian satellites(de Pater et al. 1997) .
- The synchrotron spectrum is relatively flat (see Fig. 1) over a wide range of frequencies and peaks at a maximum frequency $\nu_{max} \propto E^2 B$ with ν_{max} in MHz, B in Gauss and E the energy of electrons in MeV (Dessler 2002b). The resulting spectrum is the superimposition of all spectra received from different electron populations (at different energy E) located at different distances from the planet (i.e with different B).
- This emission is continuous and relatively stable at very short term (few min) as compared to the sporadic DAM emissions at lower frequencies. The received power, projected on the sky, is the accumulation of the emission along the observer line of sight. The planetary rotation will therefore induce the variation of the location of the "piercing" points and that of the optical path through the optically thin radiation belts. As a consequence, the extended emission projected on the sky varies notably at timescales of ~ 30 (corresponding to a planetary longitude variation of $\sim 18^o$, referred to as the Central Meridian Longitude (CML) in the system III (1965) coordinate system (Dessler 2002a)). In addition to this apparent variability, intrinsic temporal variations were observed at times scales from few days Santos-Costa et al. (2009) to years (de Pater & Klein 1989). The origins of these variations are multiple and were attributed to diffusion processes occurring inside the belts (de Pater & Goertz 1994; Tsuchiya et al. 2011), variation of the solar wind properties (de Pater & Goertz 1994), interaction with galilean satellites or caused by impact events (Brecht et al. 2001; Santos-Costa et al. 2011).

The radio emissions mapping of Jupiter radiation belts improved by using large interferometers such as the WSRT, the ATCA and the VLA. As a proxy for the distribution of electrons, it led to the development of advanced models (see de Pater (1981); de Pater & Sault (1998); Santos-Costa et al. (2001)). By confirming the observed emission, these models enabled the identification of the source and mode of transport of the electron populations in Jupiter radiation belts. Not much is known about the low ($\lesssim$200 MHz) and high ($\gtrsim$ 10 GHz) frequency components of the synchrotron radiation, nor about their variation with time. The knowledge of these properties is of great importance to refine these models (de Pater 2004) and to formulate an accurate description of inner magnetic field of Jupiter.

2 The LOFAR Observation

With LOFAR[ii] (van Haarlem et al. 2012), we were able to make the first resolved observations at frequencies below 200 MHz. Jupiter was observed continuously during ten hours from 2011/11/10:18h24 UT to 2011/11/11:4h24 UT with LOFAR in interferometer mode configured with 49 antennas. Each antenna (or "station") is an array or a sub-array composed of High Band Antennas (HBA) which signals undergo digitization and processing that result in a virtual pointing (beamforming) toward the direction of interest. Two

[ii] www.lofar.org

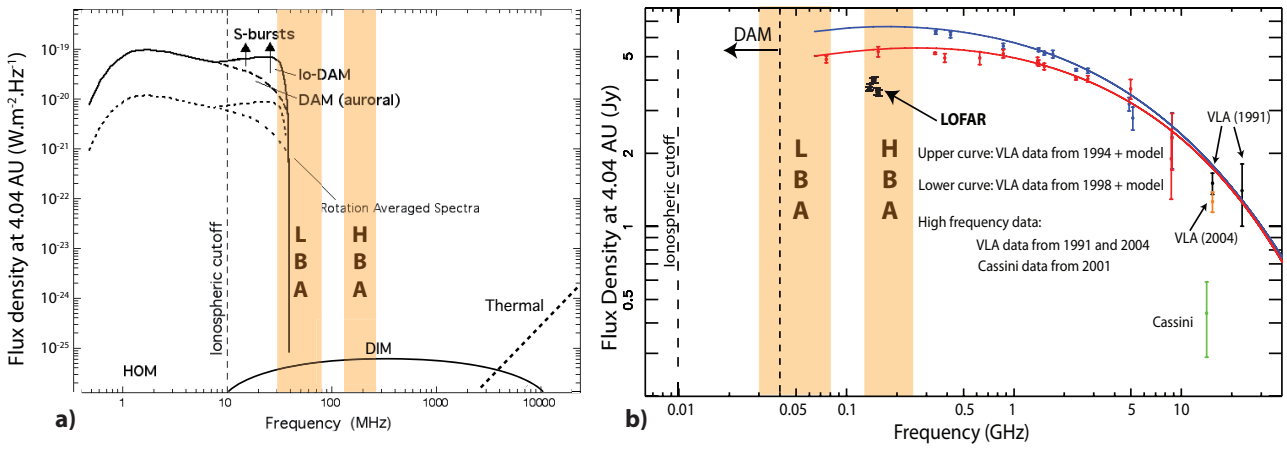

Fig. 1. The two bandwidths of the LOFAR is represented with the shaded area. The "low band antenna" (LBA) bandwidth is ≈30 to 80 MHz and the "High Band Antenna" (HBA) bandwidth is ≈120 to 240 MHz is (from `lofar.org`). **Left:** Spectrum of the existing radio emissions at Jupiter (DAM, DIM and thermal) adapted from Zarka (2004). **Right:** Measurements of the DIM emission with Cassini (2001) and the VLA measurements at three periods (1991, 1994, 1998) superimposed with models (Kloosterman et al. 2008) from 74 MHz up to 13 GHz. To account for the varying distance between Jupiter and the observer, flux densities are scaled to the standard 4.04 AU distance. LOFAR points with errors bars are the total flux density measurement on unresolved LOFAR images from 127 to 149 MHz. These error bars are computed from the RMS noise in source-free patches of the images.

numerical beams (of $\sim$ 24 MHz) were synthesized and pointed toward two directions: one was pointed toward the Jupiter mean position at the time of observation and the other toward a phase calibrator (4C15.05) situated 4^o away from Jupiter. For a total bandwidth of 47.26 MHz, 24 MHz was attributed to each beam and distributed in 121 sub-bands (SB) over [127-172] MHz. We used a high temporal and spectral resolution (dt=0.3ms x df=763Hz) to enable RFI excision before the data processing. The data are measurement sets of the visibilities between each antenna.

2.1 Data processing

Data bins polluted by RFI (representing $\approx 5-10\%$ of the data) and misbehaving stations were flagged. The data were then rebinned to dt=9.01s and df=195kHz. The first 1.5h and the last hour of the 10hrs observation were heavily polluted data. This behavior is partly due to the low elevation of the source ($\mathrm{dec}_{start} \approx 27^o$ & $\mathrm{dec}_{end} \approx 10^o$) and the local ionospheric conditions (at dusk).

The data were calibrated using the phase calibrator and the standard calibration tools provided by the LOFAR system. Since there is no specific planetary imaging mode implemented in LOFAR and no planetary tracking capability, we used the standard imaging mode (that can track source of constant RA/DEC). Indeed, in contrast to "fixed" sources that rotate with the sky (at 15^o/hr), Jupiter had an additional motion of ≈2-3' (across the beam) during a 10h observation.

Moreover, the 10^o tilt between its magnetic and rotation axes make the main radiation peaks to "wobble" of the projected image plane, as these are aligned with the magnetic equator. The magnitude of these two effects varies with the source-to-observer configuration and induces a smearing of the emission structure in resolved radio maps after long-integration. This smearing effect makes the scientific interpretation next to impossible. It is possible to know the accurate position of the planet (with ephemeris provided by JPL Horizons[iii] & IMCCE[iv]) and the geometrical configuration of the observer w.r.t. the spin & magnetic axes of the planet (Earth jovicentric latitude $D_E = 3.29^o$ in november 2011). We derived the direction and angle of projected magnetic equator containing the two radiation peaks with respect to the sky reference frame. These two major effects can be corrected by the application of rotation matrices and phase corrections coefficients directly on the visibility data at each time steps. However, the nearby sources that have constant RA/DEC coordinates will undergo an artificial smearing

[iii] `http://ssd.jpl.nasa.gov/`
[iv] `http://www.imcce.fr/fr/ephemerides/`

with these corrections. Therefore it was necessary to subtract a maximum number of background sources from the target field visibilities before applying the corrections. This stage requires a preliminary wide-field imaging (using AWimager from (Tasse et al. 2012) dealing with direction-dependent effects) around the target, the source detection, visibility simulations of these sources and their subtraction (known as "peeling"). We used a parallel source peeling algorithm on unresolved wide-field images which removed ~ 50 sources from the visibilities. The set of tools developed for these commissioning data may become the standard way to automatically process LOFAR planetary visibility data.

2.2 Preliminary results

2.2.1 Total flux measurements

We used the Cotton-Schwab (Schwab 1984) CLEAN algorithm (in a CASA environment) to image the Jupiter DIM emission. A first set of images was produced to measure the total flux in the direction of Jupiter. These images were integrated over 7hrs from 19:00 UT to 2:00 UT. On Fig. 1 (right), we added the LOFAR flux measurements (scaled to the standard 4.04 AU distance from Jupiter) to previous measurements from the VLA (adapted from Kloosterman et al. (2008)). The errors bars were computed using the RMS noise of the corresponding images in empty patches of the sky. No systematic error was evaluated here.
We measured flux densities of [3.5-4]$\pm$[$0.1-0.3$] Jy which are lower to what was obtained from tabulated values derived from models and observations (Kloosterman et al. 2008) ($\approx$5-6 Jy at these frequencies).
The variation of the spectrum shape between the two VLA datasets between 1994 and 1998 is $\sim$1-1.5 Jy and is addressed in de Pater & Dunn (2003). The LOFAR data were obtained more than 10 years after these VLA values and the flux difference observed can result from the combination of both geometrical (target-to-observer parameters, different optical paths) and the intrinsic variations of the emission at the source. Long-term (decades) variations of the DIM flux density was reported by Klein et al. (1989). Flux measurements at 13 cm taken from 1964 to 1987 were compiled and revealed flux variations of 3 Jy to 5.5 Jy ($\approx 40\%$) over the years.

2.2.2 Resolved radio maps

We have produced 12 images, each computed from 10 consecutive SB and integrated over 7hrs. We present on Fig. 2, the surface brightness obtained from the accumulation of the 12 LOFAR images over 7hr (averaged over 70% of the planet rotation). The final spatial resolutions obtained with this dataset was 17.8"-15.5" (the white ellipse represents the average CLEAN beam). We compare the obtained map to that obtained by de Pater & Dunn (2003) with VLA data at 15 GHz. We can identify the two main radiation peaks at each side of Jupiter (represented with a black circle) matching the radiation peaks from the VLA dataset. The 1-2^o misalignment is due to the different observer-to-target configurations of the two periods of observation ($D_E = 0.45^o$ in 1991 and $D_E = 3.29^o$ in 2011). The distance of the peaks from the planet center is ~ 1.3 R_j on the two datasets. No clear sign of long-term variability can be derived at this resolution between 1991 and 2011.

3 Ongoing work and perspectives

We measured for the first time, the flux density of the Jupiter DIM emission with LOFAR in the [127-149] MHz. We also produced resolved maps of the emission from [127-172] MHz by using the standard interferometer mode of LOFAR. We developed and validated a toolkit that handles the planetary imaging data with LOFAR. Advanced methods, available in the LOFAR toolkit,were used such as direction-dependent calibration, wide-field imaging at low frequencies and source peeling. With supplementary operation on the (u,v) data, we corrected for the planetary motion on the sky and the radio source wobbling.
We obtained flux levels of the same order of magnitude of that obtained with previous VLA observations with a sensitivity of $\pm$0.2 Jy. The comprehensive scientific exploitation as well as other observations with LOFAR and the VLA will be carried in the next few months. An observation proposal was submitted to answer the first Public Call for observations with LOFAR. These future observations include observations with in HBA band and in LBA band (at frequency/time where there is no dominating DAM emissions). We plan to observe several calibrators during the future observations with LOFAR (during Cycle 0). Two beams will be used, one pointing at the planet and the other pointing at a phase calibrator close to Jupiter to monitor the local conditions of the targeted area in the sky. A primary flux calibrator will also be used to bootstrap the value of flux density on a known source. In addition, a polarized calibrator will be observed from time to time during the observation to

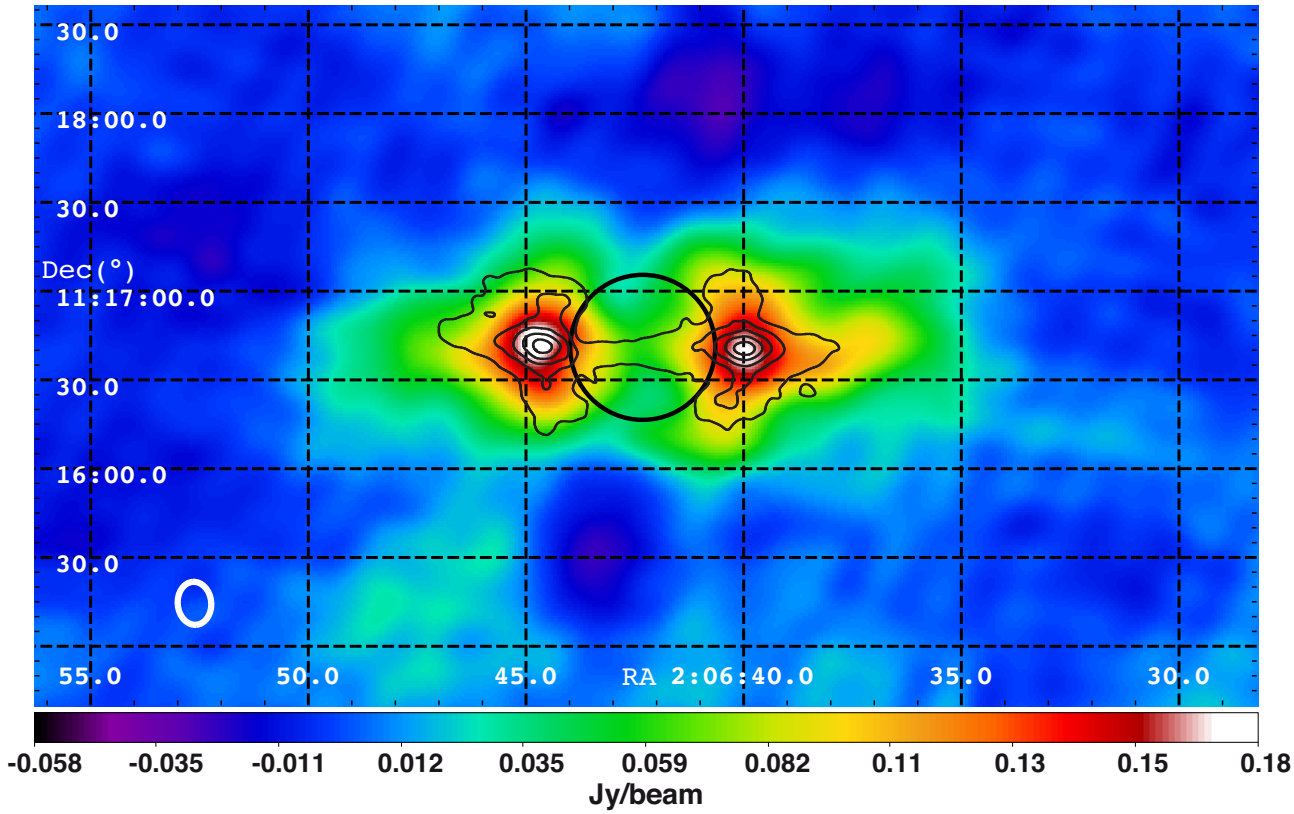

Fig. 2. The rotation-averaged image of the Jupiter radiation belts emission over 127-172 MHz is represented with the color map in celestial coordinates. The image RMS noise is 4 mJy/beam. The contours are the linearly polarized flux levels at 15 GHz from VLA data taken during March 1991 (de Pater & Dunn 2003). The black circle locates the Jupiter disk on the sky. The VLA map was scaled up to match the LOFAR data to take into account the change of Jupiter apparent size between the two dates (Jupiter was at a distance of 4.55 AU in March 1991 and 3.99 AU in november 2011). The contour interval is 3 mJy/beam and starts at 2 mJy/beam.

monitor the change of polarization due to the ionospheric & instrumental effects. The polarization information of these emissions are decisive, especially that of the circular component of the radiation. If measured, it will provide much information on the non-dipolar character of Jupiter magnetic field (de Pater 1981). Estimates indicate that the 5-10 mJy level of the circular component may just be in the scope of LOFAR detectability (1-10 mJy). This observation was carried during the LOFAR commissioning phase. Therefore the data quality was not guaranteed, but the essential reduction tools were fully functional and enabled the advanced implementation of reduction scripts to treat planetary data. An additional set of observations covering more than two Jupiter rotations will enable:

1. the search for yearly temporal variations (2011-2013) in the LOFAR data.

2. the investigation of the polarization of the emission by combining the information from different datasets from various instrument.

3. the measurement of the total spectral content over a very wide range of frequencies from 60 MHz up to $\sim$ 14 GHz.

LOFAR, the Low Frequency Array designed and constructed by ASTRON, has facilities in several countries, that are owned by various parties (each with their own funding sources), and that are collectively operated by the International LOFAR Telescope (ILT) foundation under a joint scientific policy. The authors thank Roberto Pizzo (ASTRON, Dwigeloo) for his assistance with the raw data and Jean-Mathias Grießmeier (LPC2E, Orléans) for the observation setup. We thank the members of the LOFAR Planetary & Exoplanetary Working Group (PeWG) from the LOFAR Key Science Project: Planets & Exoplanets.

References

Brecht, S. H., de Pater, I., Larson, D. J., & Pesses, M. E. 2001, Icarus, 151, 25

Burke, B. F. & L., F. K. 1955, J. Geophys. Res., 60(2), 213

de Pater, I. 1981, J. Geophys. Res., 86, 3397

de Pater, I. 2004, Planetary and Space Science, 52, 1449

de Pater, I. & Dunn, D. E. 2003, Icarus, 163, 449

de Pater, I. & Goertz, I. 1994, J. Geophys. Res., 99, 2271

de Pater, I. & Klein, M. J. 1989, NASA Special Publication, 494, 139

de Pater, I. & Sault, R. J. 1998, J. Geophys. Res., 103, 19973

de Pater, I., Schulz, M., & Brecht, S. H. 1997, J. Geophys. Res., 102, 22043

Dessler, A. 2002a, Physics of the Jovian Magnetosphere, Vol. 3 of Cambridge Planetary Science Series (Cambridge University Press), 498–504

Dessler, A. 2002b, Physics of the Jovian Magnetosphere, Vol. 3 of Cambridge Planetary Science Series (Cambridge University Press), 231–250

Klein, M. J., Thompson, T. J., & Bolton, S. 1989, NASA Special Publication, 494, 151

Kloosterman, J. L., Butler, B., & de Pater, I. 2008, Icarus, 193, 644

Mayer, C. H., McCullough, T. P., & Sloanaker, R. M. 1958, ApJ, 127, 11

Roberts, J. A. 1976, Proceedings of the Astronomical Society of Australia, 3, 53

Santos-Costa, D., Bolton, S. J., & Sault, R. J. 2009, A&A, 508, 1001

Santos-Costa, D., Bolton, S. J., Sault, R. J., Thorne, R. M., & Levin, S. M. 2011, Journal of Geophysical Research (Space Physics), 116, 12236

Santos-Costa, D., Sault, R., Bourdarie, S., et al. 2001, Advances in Space Research, 28, 915

Schwab, F. R. 1984, AJ, 89, 1076

Tasse, C., van der Tol, B., Bhatnagar, S., van Diepen, G., & van Zwieten, J. 2012, in prep

Treumann, R. 2006, Astronomy and Astrophysics Review, 13, 229

Tsuchiya, F., Misawa, H., Imai, K., & Morioka, A. 2011, Journal of Geophysical Research (Space Physics), 116, 9202

van Haarlem, M. P., Wise, M. W., Gunst, A., et al. 2012, A&A, submitted

Wu, C. S. & Lee, L. C. 1979, ApJ, 230, 621

Zarka, P. 2004, Planet. Space Sci., 52, 1455

Zarka, P. 2004, Advances in Space Research, 33, 2045